SEMARAK ILMU PUBLISHING

CFD Letters

Journal homepage:
https://semarakilmu.com.my/journals/index.php/CFD_Letters/index
ISSN: 2180-1363

Numerical Investigation into Laminar-Flow-Sensitive Aerodynamic Behavior of the NACA 0012 Airfoil at Subsonic Mach Numbers

Ayush Kamboj[1*]

1. Ayush	1. Kamboj	1. mdkayushkamboj@gmail.com

[1] Faculty of Engineering, and Applied Sciences, Cranfield University, Bedford, United Kingdom

ARTICLE INFO

Article history:
Received 29 October XXXX
Received in revised form 1 December XXXX
Accepted 9 December XXXX
Available online 10 December XXXX

Keywords:
Laminar flow, Subsonic aerodynamics, Airfoil thickness, Transition modeling, XFLR5, CFD, Pressure gradient sensitivity

ABSTRACT

Laminar flow behavior over airfoil surfaces plays a critical role in determining the aerodynamic efficiency in subsonic flight, particularly through its influence on viscous drag and boundary-layer development. The thickness of an airfoil affects the pressure-gradient distribution along the surface and can therefore influence laminar flow stability and aerodynamic performance. Quantitative investigations on isolating the thickness as an independent geometric parameter under consistent numerical conditions remain limited. This study presents a numerical investigation into the influence of airfoil thickness on laminar flow characteristics at subsonic Mach numbers. A symmetric NACA 0012 airfoil was adopted as the baseline geometry, and systematic thickness variations were introduced while maintaining a constant chord length and camber characteristics. The aerodynamic performance was analyzed using XFLR5 predictions combined with computational fluid dynamics (CFD) simulations performed using a Reynolds-averaged Navier–Stokes framework with transition-sensitive modeling. The analysis was conducted under subsonic operating conditions representative of low-speed aerodynamic applications. The results showed that increasing the airfoil thickness strengthened the adverse pressure gradients on the suction surface, leading to increased boundary-layer sensitivity and drag penalties. Thinner configurations exhibited delayed pressure recovery and improved aerodynamic efficiencies within the investigated operating range. CFD flow-field visualization further illustrated the relationship between pressure gradient development, wake growth, and aerodynamic performance trends. The findings provide insights into the sensitivity of laminar flow behavior to airfoil thickness and highlight the efficacy of the XFLR5 and CFD approaches in early-stage airfoil design and aerodynamic evaluations.

[*] *Corresponding author.*
E-mail address: mdkayushkamboj@gmail.com

https://doi.org/10.37934/cfdl.17.4.XX

1. Introduction

Laminar flow behaviour over aerodynamic lifting surfaces plays a fundamental role in determining the aerodynamic efficiency of a subsonic aircraft. Maintaining laminar boundary layers over a significant portion of an airfoil surface can reduce viscous drag and improve lift-to-drag performance, making laminar flow considerations particularly important in early-stage aerodynamic design (Anderson, 2017; Pope, 2015).

Among the geometric characteristics that influence boundary-layer behaviour, airfoil thickness has a direct impact on the pressure-gradient distribution along the surface. Thickness variations modify airfoil curvature and affect pressure recovery on the suction surface, which in turn influences laminar flow stability and transition behaviour (Ma et al., 2015; Kumar & Narayanan, 2022; Bangga et al., 2021). Thinner airfoils generally produce milder adverse pressure gradients and can sustain laminar flow over longer portions of the chord, whereas thicker airfoils tend to promote stronger pressure gradients that accelerate boundary-layer transition and increase viscous drag.

Previous investigations on airfoil aerodynamics have examined the influence of airfoil geometry using both experimental and numerical approaches. Many of these studies focused on comparisons between different airfoil families or involved simultaneous variations in geometric parameters such as camber and thickness distribution, making it difficult to isolate the independent aerodynamic influence of thickness alone (Ma et al., 2015; Bangga et al., 2021).

Numerical tools such as panel methods and computational fluid dynamics (CFD) provide an efficient framework for controlled parametric investigations in which individual geometric parameters can be systematically studied. However, relatively few studies have isolated the effect of airfoil thickness under consistent numerical conditions while maintaining geometric similarity across configurations.

This study addresses this gap by performing a controlled parametric investigation in which airfoil thickness is systematically varied while maintaining consistent geometric and numerical conditions. A symmetric NACA 0012 airfoil is used as the baseline geometry, and thickness-scaled variants are analysed under subsonic operating conditions. A dual XFLR5–CFD approach is employed to evaluate aerodynamic performance and provide flow-field interpretation of pressure distribution, boundary-layer behaviour, and wake development.

The objective of this study is to understand how airfoil thickness influences laminar-flow-sensitive aerodynamic performance and to demonstrate the effectiveness of combined numerical approaches for early-stage airfoil analysis.

2. Numerical Methodology

2.1 Governing Equations and Solver Framework

The aerodynamic flow around the airfoils was modeled using steady-state compressible Reynolds-averaged Navier–Stokes (RANS) equations. Mass, momentum, and energy were conserved using a pressure-based finite-volume framework. Spatial discretization was performed using second-order accuracy schemes to reduce numerical diffusion and improve the fidelity of the surface pressure and boundary-layer predictions.

The continuity equation is given by:

$$\frac{\partial \rho}{\partial t} + \nabla \cdot (\rho u) = 0$$

The momentum conservation equation is expressed as:

$$\frac{\partial(\rho u)}{\partial t} + \nabla \cdot (\rho u u) = -\nabla p + \nabla \cdot \tau$$

The aerodynamic performance was evaluated using the lift and drag coefficients, defined as:

$$C_L = \frac{L}{\frac{1}{2} \cdot \rho V^2 A}$$

$$C_D = \frac{D}{\frac{1}{2} \cdot \rho V^2 A}$$

The pressure distribution over the airfoil surface was analyzed using the pressure coefficient:

$$C_p = \frac{p - p_\infty}{\frac{1}{2} \cdot \rho V_\infty^2}$$

where ρ is the fluid density, u is the velocity vector, p is the static pressure, τ is the viscous stress tensor, V is the freestream velocity, V_∞ is the freestream velocity at infinity, and A is the reference area.

Simulations were conducted under subsonic flow conditions with freestream properties specified according to the selected Mach and Reynolds numbers. Convergence was assessed through a combination of residual reduction and stabilization of the integrated aerodynamic coefficients. Solutions were considered converged once the residuals of all the governing equations decreased below 10^{-5} and the aerodynamic force coefficients (lift and drag) exhibited stable values over successive solver iterations.

The numerical simulations were performed using a pressure-based solver in ANSYS Fluent software. The governing RANS equations were solved using a steady-state formulation appropriate for the investigated subsonic operating conditions. Spatial discretization of the momentum and energy equations was performed using second-order accurate schemes to improve the resolution of the pressure gradients and boundary-layer behavior around the airfoil surface. Pressure–velocity coupling was handled using the SIMPLE algorithm.

2.2 Transition Modeling Approach

To capture the laminar–turbulent transition behavior within the boundary layer, the γ–Re_ϑ transition shear stress transport (SST) model available in ANSYS Fluent was employed. This model combines the SST *k*–*ω* turbulence model with two additional transport equations governing intermittency (γ) and the transition momentum thickness Reynolds number (Re_ϑ). This model enables improved predictions of the laminar-to-turbulent transition behavior in aerodynamic boundary layers and has been widely applied in airfoil flow simulations (Ruiz & D'Ambrosio, 2022; Matyushenko et al., 2018).

Transition prediction within RANS-based models is inherently approximate and sensitive to modeling assumptions. Consequently, the transition model was used to capture the relative trends in the laminar flow development and drag characteristics rather than to predict the exact transition onset locations. This treatment is considered appropriate for a controlled parametric investigation focused on thickness sensitivity under consistent numerical conditions. The γ–Reθ transition SST approach has also shown improved aerodynamic prediction capability for NACA-series airfoils under low-Reynolds-number conditions (Khan et al., 2020).

2.3 Computational Domain

A 2D computational domain was constructed around each airfoil to efficiently resolve the near-wall flow physics while maintaining a manageable computational cost. An open C-type domain topology was employed to allow undisturbed inflow development and stable wake formation downstream of the airfoil.

The computational domain was constructed such that the far-field boundaries were positioned approximately 15 chord lengths (15*c*) away from the airfoil surface in all directions to minimize boundary interference and blockage effects. The downstream boundary was extended to approximately 20 chord lengths to ensure stable wake development and prevent artificial reflection of disturbances from the outlet boundary. The same domain extent was used for all the airfoil configurations to ensure direct comparability between the cases.

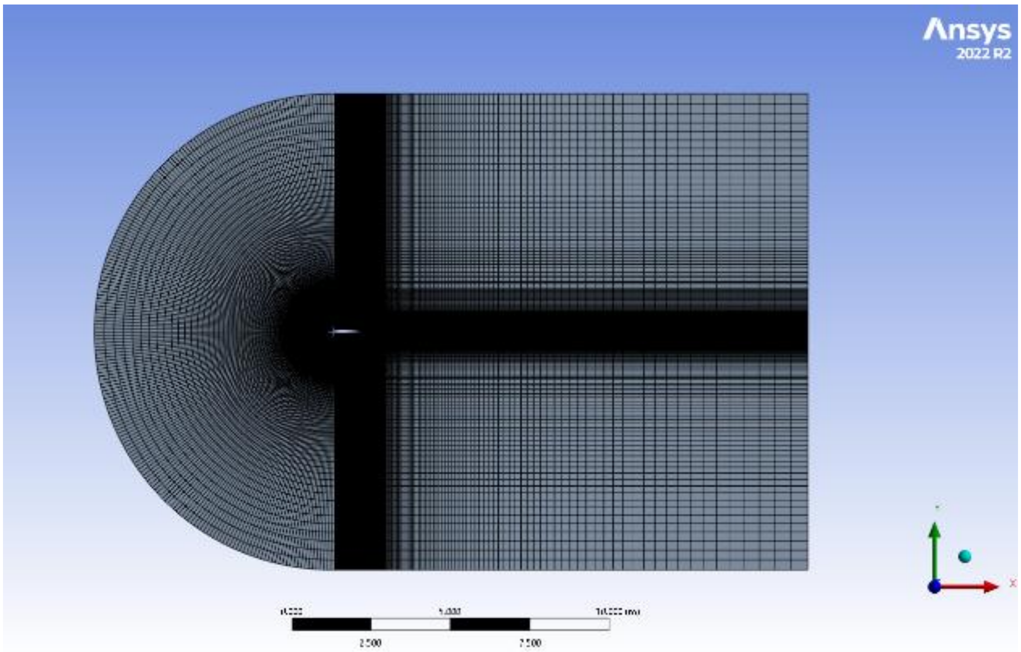

Fig. 1 Two-dimensional C-type computational domain used for airfoil simulations.

2.4 Mesh Generation and Near-Wall Resolution

Structured quadrilateral meshes were generated within the computational domain, with strong clustering near the airfoil surface to accurately resolve boundary-layer development. Local refinement was applied near the leading and trailing edges, where the surface curvature and pressure gradients were most pronounced.

Near-wall mesh spacing was selected to maintain low nondimensional wall distances throughout the simulations, ensuring adequate resolution of the laminar and transitional boundary layers. The mesh topology, growth rates, and refinement strategy were kept consistent across the thickness configurations so that the observed aerodynamic differences could be attributed primarily to geometric variations rather than numerical artifacts.

Figures 2 and 3 show the representative mesh topology and grid quality.

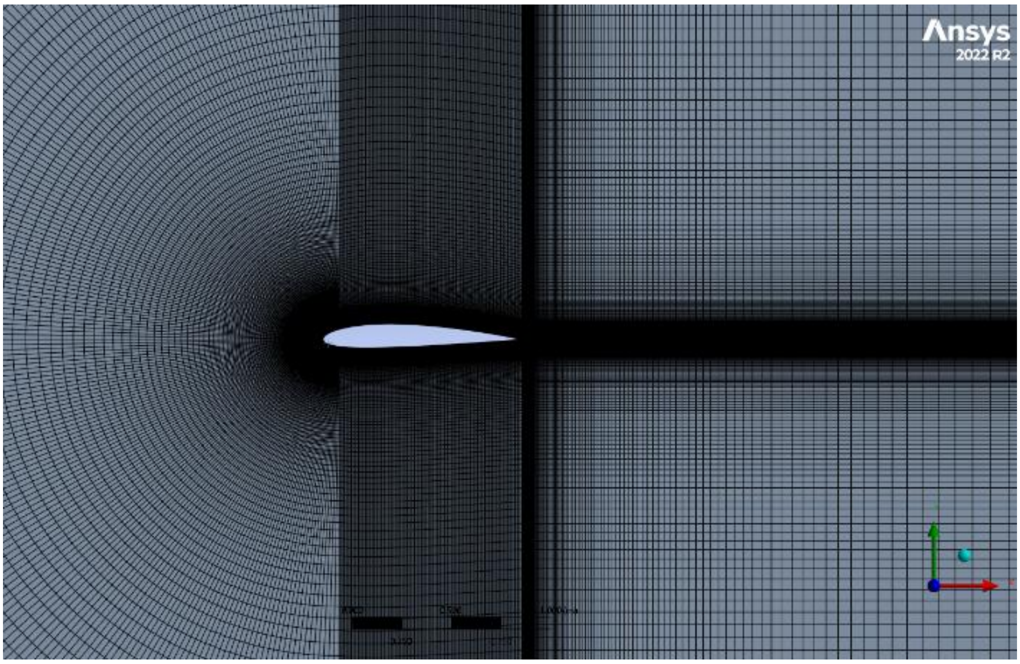

Fig. 2 Structured mesh topology around the airfoil surface.

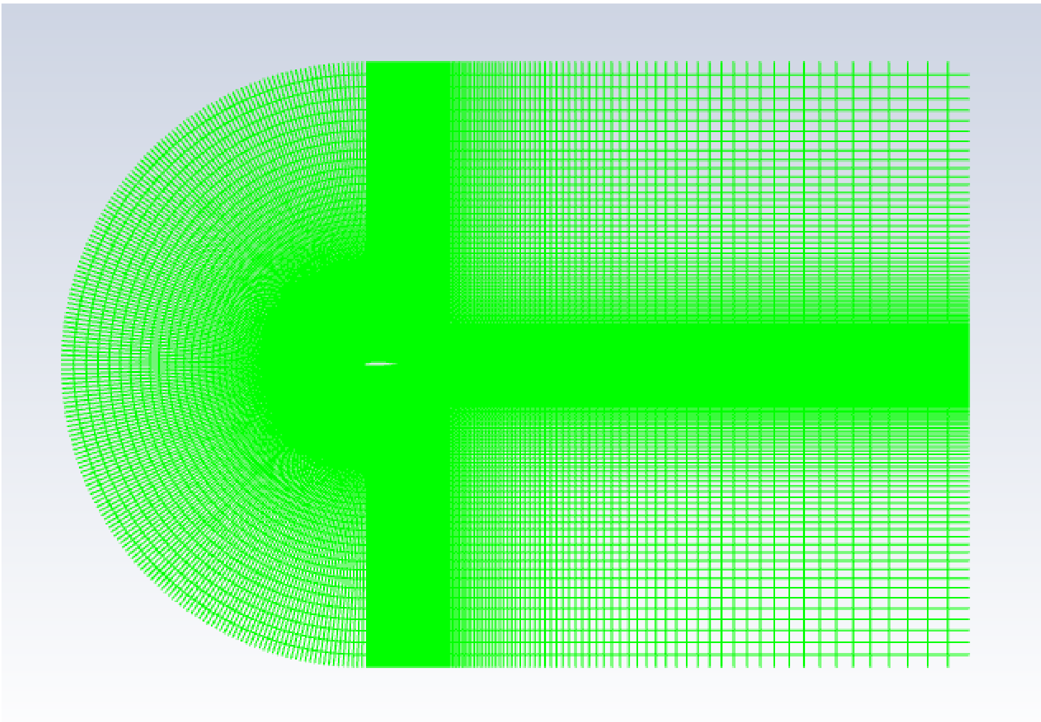

Fig. 3 Near-wall mesh refinement and boundary-layer resolution.

Mesh refinement was applied near the leading and trailing edges where strong pressure gradients were present (Douvi et al., 2010; Shah et al., 2015). The first near-wall cell height was selected to maintain a nondimensional wall distance of $y+ < 1$, allowing for an accurate resolution of the laminar and transitional boundary layers (Zidane et al., 2017; Douvi et al., 2010). The final computational mesh comprised approximately 150,000–165,000 cells, providing an appropriate balance between numerical accuracy and computational efficiency.

2.5 Boundary Conditions and Operating Parameters

Uniform freestream conditions were applied at the far-field boundaries, corresponding to the prescribed subsonic Mach and Reynolds numbers. A pressure outlet condition was imposed downstream to allow natural wake development. The airfoil surface was modeled as a no-slip adiabatic wall.

The angle of attack was imposed by adjusting the freestream flow direction relative to the airfoil chord line. All the simulations were conducted under steady-state assumptions, which were considered appropriate for subsonic operating conditions and pre-stall angles of attack. Identical boundary condition formulations were applied across all the cases to preserve numerical consistency.

2.6 Grid Independence Assessment

A grid-independence assessment was conducted to ensure that the numerical results were not excessively influenced by the mesh resolution. Mesh refinement studies were performed for a representative baseline configuration by progressively increasing the mesh density while monitoring key aerodynamic quantities, including lift and drag coefficients and surface pressure distributions.

The mesh resolution was selected once further refinement resulted in negligible changes in these quantities, thereby confirming that the numerical solution was independent of the mesh resolution for the present parametric analysis. This approach ensures a balance between numerical accuracy and computational efficiency and is considered sufficient for identifying the relative aerodynamic trends associated with thickness variation.

2.7 Numerical Validation

To establish confidence in the computational framework, selected CFD results were compared with independent aerodynamic predictions obtained using XFLR5 under identical flow conditions. Comparisons of the lift coefficients and surface pressure distributions for the baseline cases showed a good agreement within the limitations of the respective modeling approaches.

While this comparison cannot replace experimental validation, it provides an independent numerical reference and supports the suitability of the adopted methodology for a comparative analysis of laminar flow behavior under subsonic conditions (Harris, 1981; Critzos et al., 1955).

2.8 Modeling Scope and Limitations

The numerical methodology was restricted to 2D flows and idealized surface conditions. Three-dimensional effects, such as spanwise pressure gradients, crossflow instabilities, and surface roughness, were not considered. These limitations are consistent with the objective of this study, which was to examine the sensitivity of airfoil-level laminar flow to thickness variation under controlled conditions.

Within this defined scope, the numerical framework is considered suitable for identifying the relative aerodynamic trends and providing design-oriented insights for early-stage airfoil analysis.

3. Test Cases and Parameters

3.1 Airfoil Selection and Thickness Variation

This study was designed to examine the sensitivity of laminar flow behavior to airfoil thickness under subsonic conditions. To isolate the thickness effects without introducing camber-induced pressure gradient variations, a symmetric airfoil was selected as the baseline geometry. The NACA 0012 airfoil was adopted for this purpose because of its well-documented aerodynamic characteristics and frequent use as a reference in numerical airfoil studies (Critzos et al., 1955; Gregory & O'Reilly, 1973; Harris, 1981).

Using a single airfoil family ensures geometric consistency across the parametric investigation and allows attributing any variations in aerodynamic behavior primarily to thickness variations rather than to differences in camber or design intent. This controlled approach is particularly important for laminar-flow-sensitive analyses, where multiple geometric parameters can influence boundary-layer development.

For the geometric context, a comparison of representative NACA airfoil geometries is shown in Fig. 4, illustrating the differences in thickness distribution and camber among commonly used profiles. This figure is included solely to provide a background on typical airfoil geometries and is not representative of the parametric test cases analyzed in this study, which were based exclusively on thickness-scaled variants of the NACA 0012 airfoil.

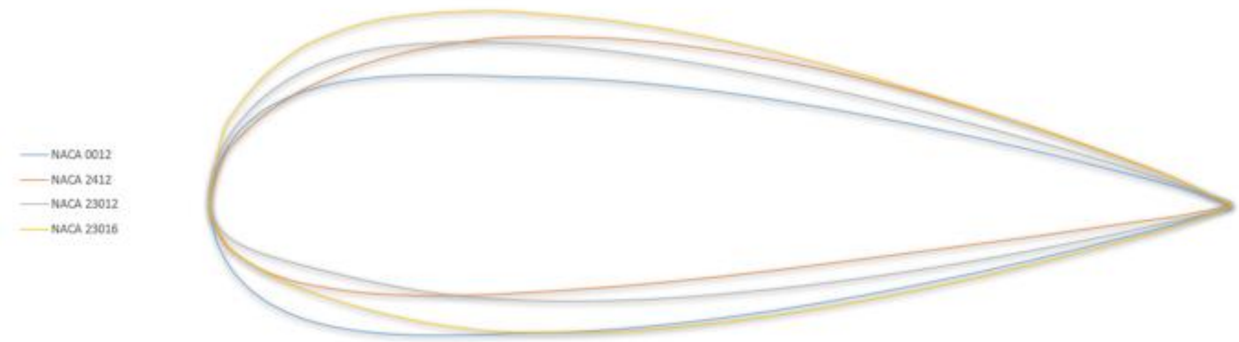

Fig. 4 Comparison of representative NACA airfoils geometries illustrating differences in thickness distribution and camber.

3.2 Thickness Modification Strategy

The thickness variation was introduced by uniformly scaling the thickness distribution of the baseline NACA 0012 airfoil, while preserving the original chord length, leading-edge position, and trailing-edge geometry. This approach maintains geometric similarity and avoids introducing secondary aerodynamic effects associated with camber modifications or planform changes.

Both the reduced- and increased-thickness configurations were considered to examine the laminar-flow sensitivity across a representative geometric range. The thickness-to-chord ratio (*t/c*) was used as the primary geometric parameter for comparison, enabling a direct assessment of the influence of thickness on pressure-gradient development, boundary-layer response, and transition behavior under identical flow conditions.

Fig. 5 shows the definition of airfoil thickness and its measurement relative to the chord line.

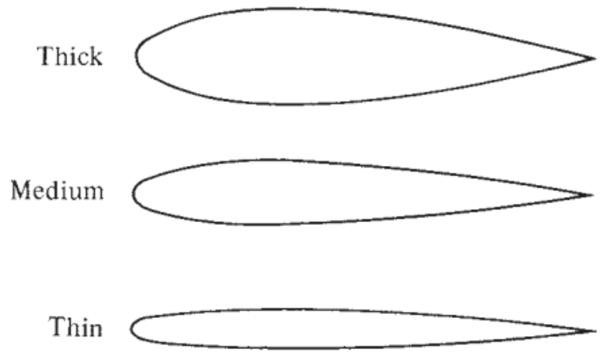

Fig. 5 Definition of airfoil thickness-to-chord ratio (t/c).

Table 1 presents a summary of the airfoil configurations investigated in this study. This condensed table replaces the detailed coordinate listings presented in the original thesis and is sufficient for describing the parametric setup for reproducibility.

Table 1 Airfoil configurations and corresponding thickness-to-chord ratios.

Configuration ID	**Baseline Airfoil**	**Thickness Scaling Factor**	**Maximum Thickness (%*c*)**	**Camber**	**Notes**
T090	NACA 0012	0.90 T	10.8	Symmetric	Reduced-thickness configuration
T100 (Baseline)	NACA 0012	1.00 T	12.0	Symmetric	Reference configuration
T110	NACA 0012	1.10 T	13.2	Symmetric	Maximum thickness investigated

3.3 Operating Conditions and Test Matrix

All the airfoil configurations were evaluated under subsonic flow conditions representative of low-speed aerodynamic applications, for which laminar flow and transition effects are expected to play a significant role. The simulations were conducted over a range of angles of attack selected to capture the linear lift behavior and onset of nonlinear aerodynamic effects while remaining within the pre-stall regime.

The Reynolds numbers were selected based on the chord length such that viscous effects and boundary-layer behavior had a measurable influence on the aerodynamic performance. Each thickness configuration was analyzed using identical sets of Mach numbers, Reynolds numbers, and angles of attack to ensure direct comparability across the test matrix.

XFLR5 analyses were employed for the preliminary assessment and numerical validation, whereas CFD simulations provided a detailed resolution of the flow field and boundary-layer behavior. Table 2 presents a consolidated summary of the operating conditions and numerical parameters for both the approaches.

Table 1 Summary of operating conditions and numerical parameters.

Parameter	XFLR5 Analysis	CFD (ANSYS Fluent) Analysis	Notes
Flow regime	Subsonic	Subsonic	All cases with $M < 0.6$
Mach number, M	0.0, 0.6	0.6	CFD focused on the compressible subsonic regime
Reynolds number, Re	$5.0{\times}10^5$	$5.0{\times}10^5$	Based on chord length
Angle of attack, α (°)	−5 to 12	−5 to 15	CFD limited to pre-stall regime
Flow model	Inviscid + viscous (panel/BL)	RANS + transition model	Method-specific
Transition treatment	Empirical (XFOIL-based)	Transition-sensitive RANS	No fixed transition location
Spatial discretization	Panel method	Finite-volume, 2nd order	CFD accuracy control
Simulation dimensionality	2D	2D	Airfoil-level analysis
Wall condition	No-slip	No-slip, adiabatic	Consistent viscous treatment
Mesh resolution	—	$y^+ < 1$	Boundary-layer resolution
Convergence criterion	—	Residuals < 10^{-5}	Force coefficient stabilization

3.4 Scope and Modeling Considerations

The analysis was restricted to 2D flow and idealized surface conditions to focus on the aerodynamic influence of airfoil thickness in laminar-flow-sensitive subsonic regimes. Three-dimensional effects, such as spanwise pressure gradients, crossflow instabilities, and surface roughness, were outside the scope of the present investigation.

Identical numerical settings, boundary condition formulations, and solver controls were applied across all cases to preserve methodological consistency. Within this controlled framework, the results presented in the following section are intended to provide comparative insights into the sensitivity of thickness-driven laminar flow, rather than an absolute prediction of the transition onset.

4. Results and Discussion

This section presents the aerodynamic performance trends obtained from the XFLR5 analysis, along with the CFD-based flow field interpretation. The results are organized to first examine the baseline aerodynamic behavior of the NACA 0012 airfoil under subsonic conditions, followed by an analysis of the aerodynamic efficiency and flow-field characteristics relevant to the laminar-flow-sensitive performance.

The results are presented in the following sections. The aerodynamic performance trends were first analyzed using XFLR5 predictions to quantify the lift, drag, and aerodynamic efficiency under subsonic conditions. Subsequently, the selected CFD flow field results were examined to provide a qualitative physical interpretation of the laminar flow behavior, pressure gradient development, and boundary layer response. This combined approach enables a robust interpretation of thickness-sensitive aerodynamic trends while remaining consistent with the modeling scope defined in Section 2.

4.1 Lift Characteristics of the Baseline Airfoil

Fig. 6 shows the variation in the lift coefficient with the angle of attack for the NACA 0012 airfoil for Mach numbers M = 0.0 and M = 0.6 at $Re = 5\times10^5$.

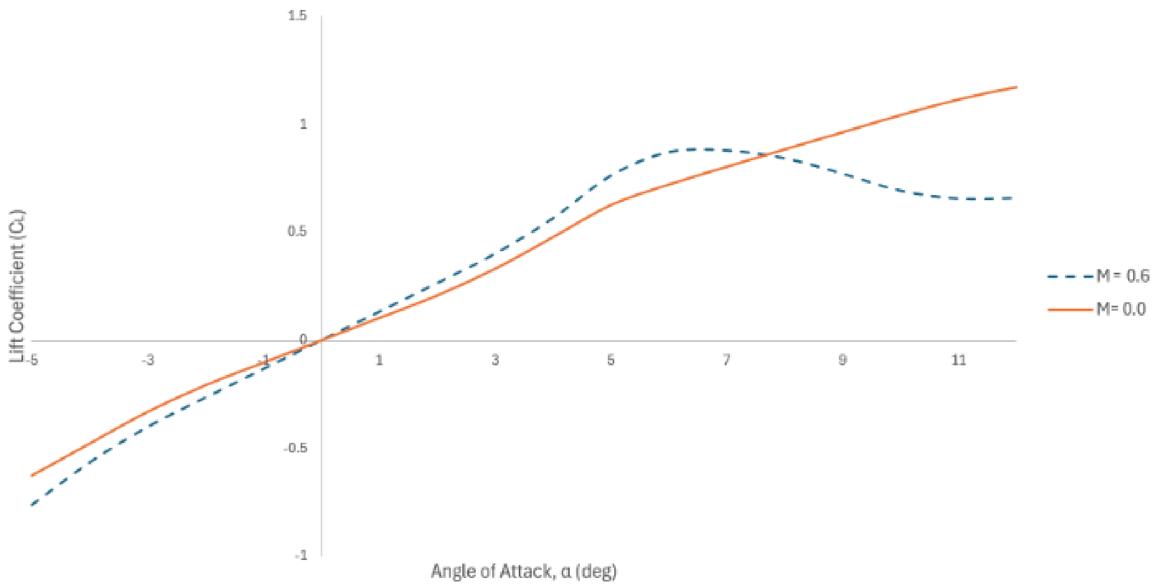

Fig. 1 Variation in the lift coefficient with the angle of attack for the NACA 0012 airfoil at $Re = 5\times10^5$ under subsonic conditions, comparing incompressible (M = 0.0) and compressible (M = 0.6) cases, obtained using XFLR5.

For both Mach numbers, the lift response remained approximately linear over the investigated pre-stall range.

At low angles of attack, the lift slopes for both cases were comparable, reflecting similar circulation development and effective camber. With increasing angle of attack, the M = 0.6 case exhibited an earlier deviation from linearity and reduced lift growth compared with the incompressible case. This behavior is consistent with the compressibility effects and increased sensitivity of the boundary layer to adverse pressure gradients at higher Mach numbers.

The absence of abrupt lift degradation within the analyzed range supports the assumption of a steady 2D flow adopted in the numerical methodology.

4.2 Drag Characteristics

Fig. 7 shows the variation in the drag coefficient with respect to the angle of attack. At low angles of attack, both the Mach number cases exhibited minimum drag near α ≈ 0°, which is characteristic of symmetric airfoils operating under laminar-flow-sensitive conditions.

With increasing angle of attack, the drag increased gradually for M = 0.0, reflecting the increasing viscous losses and mild pressure-gradient effects. In contrast, the M = 0.6 case demonstrated a substantially steeper drag increase beyond moderate angles of attack. This trend indicated stronger adverse pressure gradients, compressibility-induced effects, and reduced laminar flow stability (Chang et al., 2022; Jha et al., 2018).

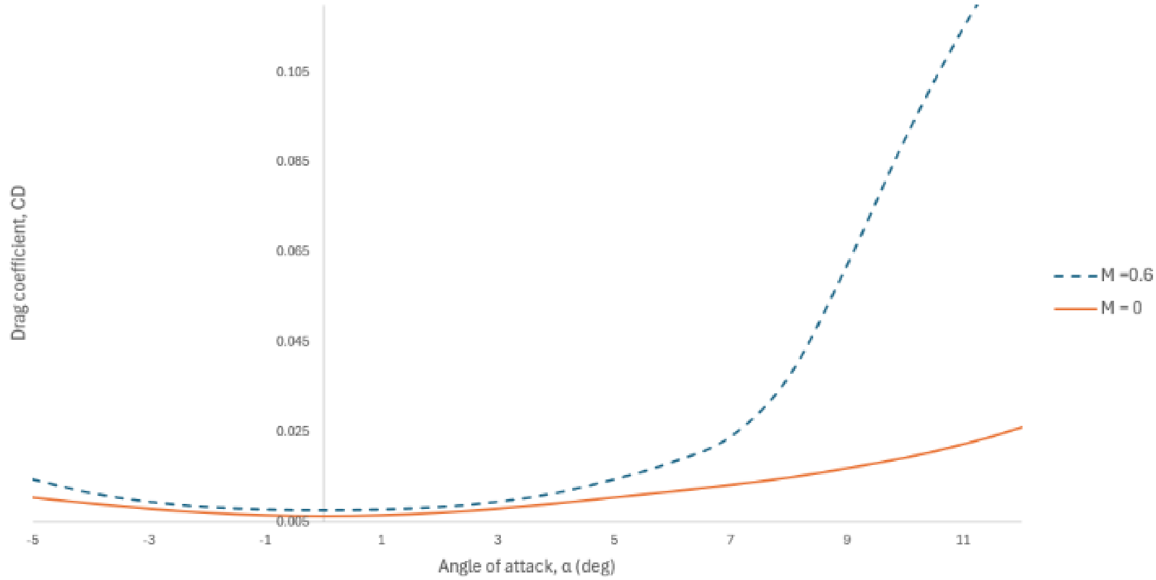

Fig. 2 Drag coefficient variation with the angle of attack for the NACA 0012 airfoil at Re = 5×10^5 under subsonic conditions for Mach numbers M = 0.0 and M = 0.6, illustrating the sensitivity of drag behavior to compressibility effects.

Although the drag values were derived from the XFLR5 predictions and should be interpreted comparatively rather than absolutely, the consistent separation between the curves clearly demonstrates the sensitivity of the drag behavior to the Mach number under otherwise identical conditions.

4.3 Aerodynamic Efficiency

The combined influence of lift and drag variations was evaluated using the lift-to-drag ratio, as shown in Fig. 8. For both the Mach numbers, the aerodynamic efficiency increased rapidly at low angles of attack and reached a maximum within the range $\alpha \approx 4°–6°$, corresponding to efficient lift generation with limited drag penalty.

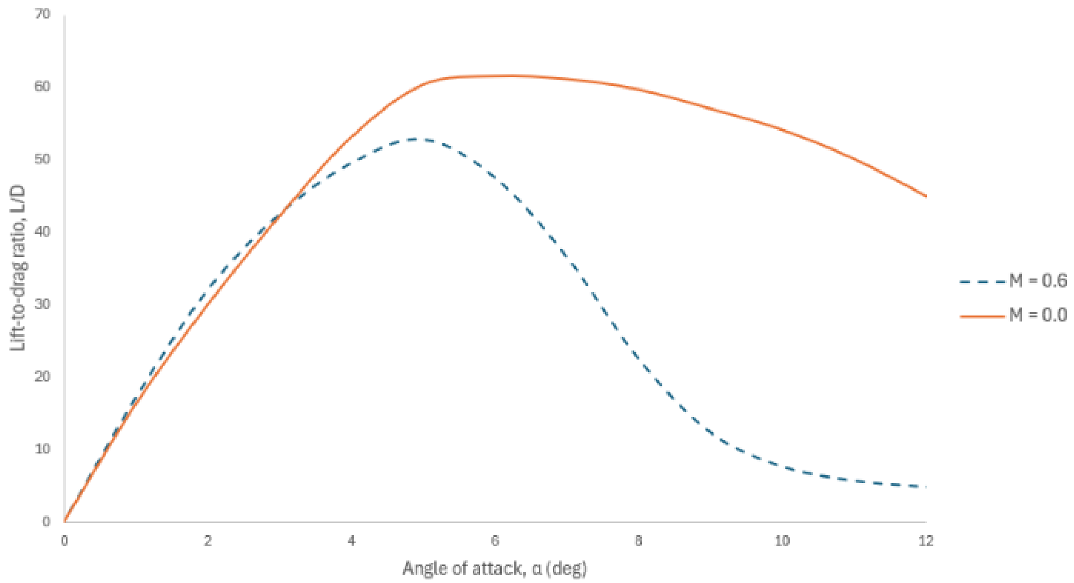

Fig. 3 Lift-to-drag ratio as a function of the angle of attack for the NACA 0012 airfoil at *Re* = 5×10^5 under subsonic conditions, derived from the XFLR5 lift and drag predictions, highlighting the variation in the aerodynamic efficiency with Mach number.

The incompressible case (M = 0.0) achieved a higher peak lift-to-drag ratio and maintained elevated efficiency over a broader angle-of-attack range. In contrast, M = 0.6 case exhibited a lower peak efficiency and a more rapid decline at higher angles of attack. This behavior directly reflects the accelerated drag increase observed in Fig. 7 and highlights the sensitivity of the laminar flow-dependent performance to compressibility effects.

Table 2 Summary of peak aerodynamic efficiency for the NACA 0012 airfoil obtained from the XFLR5 analysis under subsonic conditions (*Re* = 5×10^5). The table reports the maximum lift-to-drag ratio and the corresponding angle of attack for Mach numbers M = 0.0 and M = 0.6.

Airfoil	**Mach number**	**Reynolds number**	**Peak L/D**	**Angle of attack at Peak L/D**
NACA 0012	0.0	5×10^5	60.36	5°
NACA 0012	0.6	5×10^5	52.77	5°

The results indicate that the compressibility effects reduce the aerodynamic efficiency by approximately 12.6% as the peak lift-to-drag ratio decreases from 60.36 M = 0.0 to 52.77 M = 0.6.

4.4 Influence of Airfoil Thickness

To investigate the influence of the airfoil thickness on the laminar-flow-sensitive aerodynamic behavior, an additional parametric analysis was conducted by scaling the thickness of the baseline NACA 0012 airfoil. Three configurations were considered: a thinner airfoil with 90% baseline thickness (T090), a baseline NACA 0012 airfoil (T100), and a thicker configuration with 110% thickness (T110). All the configurations were analyzed using XFLR5 at a Reynolds number of $Re = 5 \times 10^5$ and Mach number $M = 0.6$ with $N_{crit} = 9$, ensuring consistent aerodynamic conditions for comparison. While the parametric thickness study was evaluated using XFLR5, high-fidelity CFD flow-field visualization was performed for the baseline NACA 0012 configuration to provide a qualitative physical interpretation of the underlying flow behavior, pressure gradients, and wake development at M = 0.6.

Fig. 9 shows the variation in the lift coefficient with the angle of attack for the three airfoil thickness configurations. The results indicate that decreasing the airfoil thickness slightly increased the lift coefficient at moderate angles of attack. For example, at $\alpha = 4°$, the thinner configuration (T090) produced a lift coefficient of approximately $C_L = 0.603$, compared with $C_L = 0.565$ for the baseline airfoil and $C_L = 0.530$ for the thicker configuration (T110). This behavior is associated with the modification of the pressure-gradient distribution along the suction surface, which affects boundary-layer development.

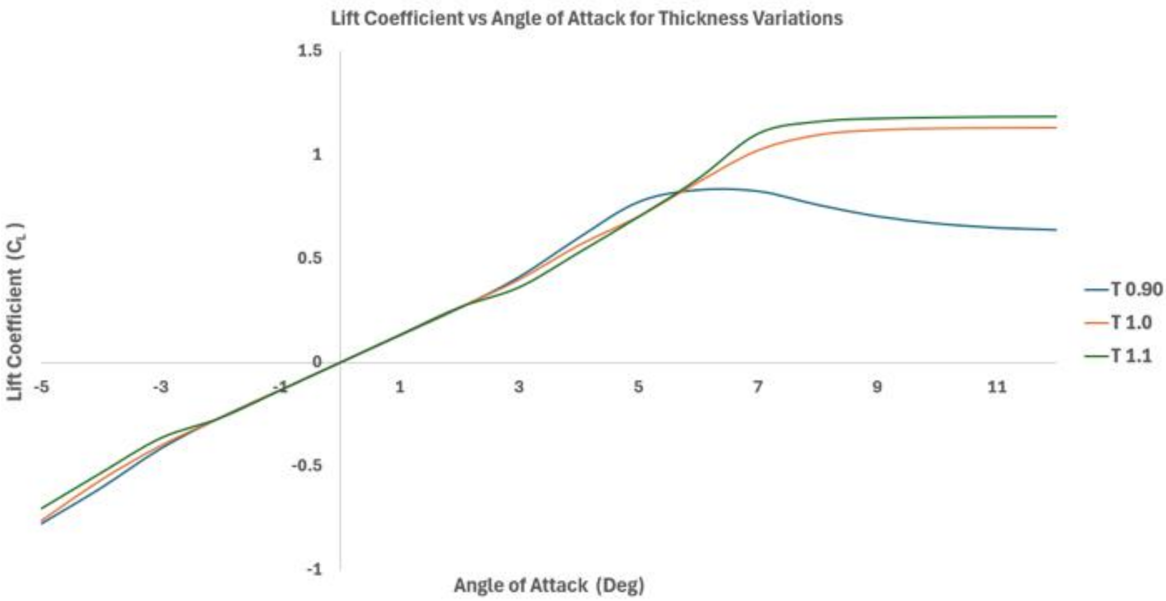

Fig. 4 Lift coefficient variation with the angle of attack for airfoil thickness configurations T090, T100, and T110 at *Re* = 5×10^5 and M = 0.6.

Fig. 10 shows the drag characteristics of the three configurations. The results indicate that the drag varied moderately with airfoil thickness. The thinner airfoil configuration generally exhibited slightly higher drag values at moderate angles of attack owing to the stronger adverse pressure gradients along the suction surface. For example, at $\alpha = 4°$, the drag coefficient for the thinner configuration was $C_D \approx 0.0119$, compared with $C_D \approx 0.0114$ for the baseline airfoil and $C_D \approx 0.0112$ for the thicker configuration.

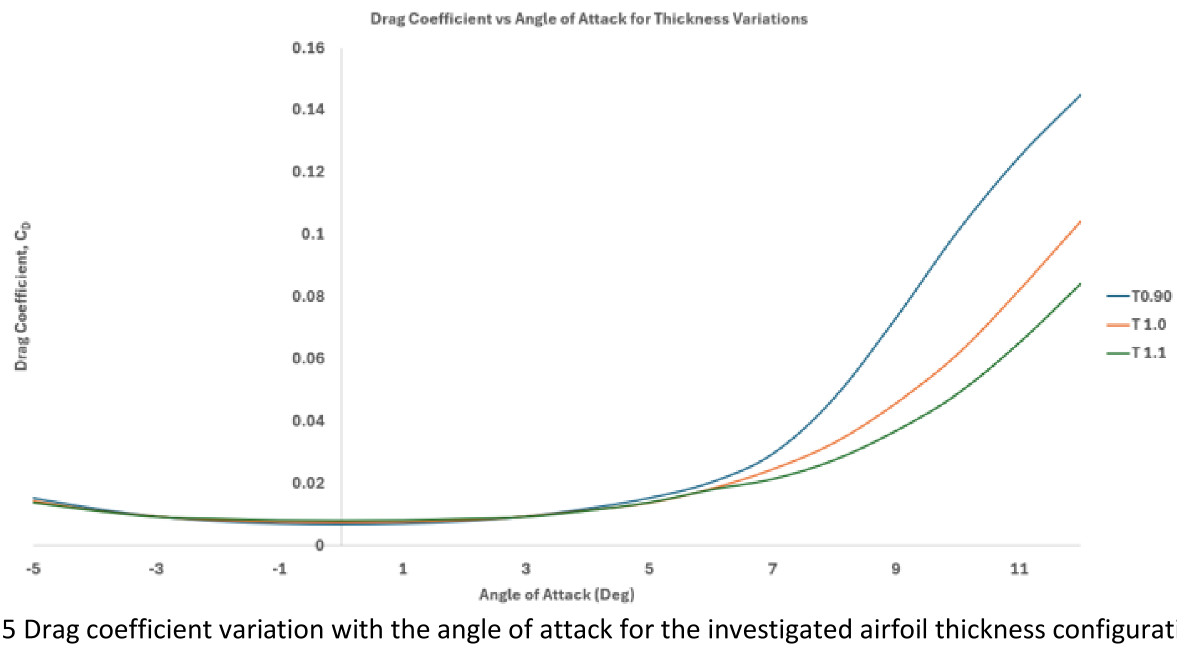

Fig. 5 Drag coefficient variation with the angle of attack for the investigated airfoil thickness configurations under subsonic conditions.

Fig. 11 shows the resulting aerodynamic efficiencies, expressed as lift-to-drag ratios. Although the aerodynamic efficiency remains relatively similar across the investigated thickness range, the thinner configuration generally provides slightly higher lift-to-drag ratios owing to the increased lift generation. At $\alpha = 4°$, the thinner configuration achieved $L/D \approx 50.7$, compared with $L/D \approx 49.6$ for the baseline airfoil and $L/D \approx 47.5$ for the thicker configuration.

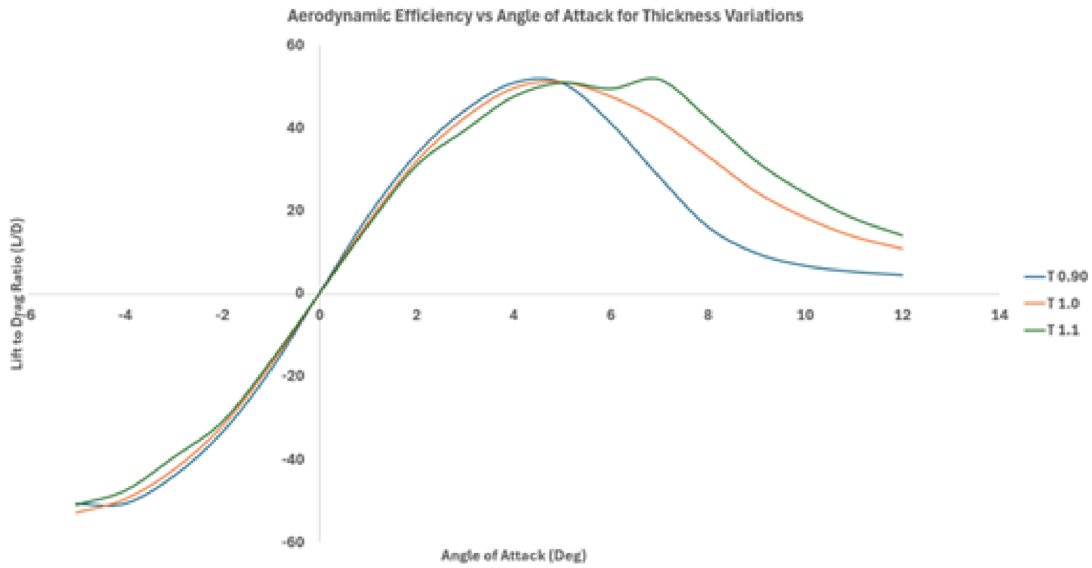

Fig. 6 Lift-to-drag ratio variation with the angle of attack illustrating the aerodynamic efficiency of different thickness configurations.

These results demonstrate that the airfoil thickness influences the aerodynamic performance primarily through its effect on the pressure gradient distribution along the suction surface. At lower angles of attack, thinner airfoils exhibited slightly improved aerodynamic efficiency owing to reduced drag levels and favorable pressure recovery characteristics. However, at higher aerodynamic loading conditions, thicker configurations demonstrated improved lift retention and lower drag growth, indicating increased resistance to adverse pressure-gradient-induced flow deterioration. Thinner airfoils tend to generate higher lifts but may experience slightly increased drag, whereas thicker airfoils produce lower lifts with marginally reduced drag levels. The combined effect resulted in relatively small variations in aerodynamic efficiency across the investigated thickness range. These trends are consistent with the classical aerodynamic theory and provide useful insights into the role of thickness variation during preliminary airfoil design studies.

Table 3 Aerodynamic performance comparison for airfoil thickness configurations T090, T100, and T110 at *Re* = 5×10^5 and M = 0.6 obtained from XFLR5 analysis.

α (°)	C_L T090	C_L T100	C_L T110	C_D T090	C_D T100	C_D T110	*L/D* T090	*L/D* T100	*L/D* T110
-5	-0.7752	-0.7612	-0.7022	0.01529	0.01442	0.01381	-50.70	-52.78	-50.85
-4	-0.6030	-0.5653	-0.5303	0.01189	0.01141	0.01117	-50.71	-49.55	-47.48
-3	-0.4132	-0.3997	-0.3629	0.00937	0.00942	0.00921	-44.09	-42.45	-39.40
-2	-0.2633	-0.2646	-0.2661	0.00785	0.00828	0.00862	-33.54	-31.96	-30.87
-1	-0.1314	-0.1324	-0.1333	0.00710	0.00773	0.00818	-18.51	-17.13	-16.30
0	0.0000	0.0000	0.0000	0.00688	0.00757	0.00806	0.00	0.00	0.00
1	0.1314	0.1324	0.1333	0.00710	0.00773	0.00818	18.51	17.13	16.30
2	0.2633	0.2646	0.2661	0.00785	0.00828	0.00862	33.54	31.96	30.87
3	0.4132	0.3997	0.3629	0.00937	0.00942	0.00921	44.09	42.45	39.40
4	0.6031	0.5653	0.5303	0.01189	0.01141	0.01117	50.72	49.55	47.48
5	0.7751	0.7036	0.7023	0.01529	0.01379	0.01381	50.69	51.01	50.85
6	0.8325	0.8696	0.8859	0.02032	0.01830	0.01794	40.97	47.51	49.38

7	0.8261	1.0226	1.1028	0.02950	0.02460	0.02136	28.00	41.56	51.63
8	0.7601	1.0962	1.1600	0.04750	0.03310	0.02750	16.00	33.11	42.18
9	0.7050	1.1200	1.1750	0.07320	0.04580	0.03690	9.63	24.46	31.85
10	0.6700	1.1280	1.1800	0.10100	0.06150	0.04880	6.63	18.34	24.18
11	0.6500	1.1300	1.1830	0.12500	0.08210	0.06520	5.20	13.77	18.14
12	0.6400	1.1310	1.1840	0.14500	0.10420	0.08430	4.41	10.86	14.04

The results indicate that decreasing the airfoil thickness slightly increases lift generation, whereas thicker configurations produce lower drag growth at higher angles of attack, leading to comparable aerodynamic efficiencies across the investigated thickness range.

At α = 4°, the thinner configuration (T090) produced approximately 6.7% higher lift than the baseline airfoil, whereas the thicker configuration (T110) produced approximately 6.2% lower lift compared with the baseline case.

4.5 Discussion

The aerodynamic trends observed in the present study are consistent with established findings in airfoil aerodynamics, particularly with respect to the role of pressure-gradient development in laminar-flow-sensitive regimes. The results indicate that airfoil thickness primarily influences aerodynamic performance through its effect on suction-side pressure gradients and boundary-layer stability.

The increase in drag with increasing airfoil thickness can be attributed to the strengthening of adverse pressure gradients along the suction surface. This behaviour promotes earlier boundary-layer transition and increased viscous losses, which is consistent with previously reported numerical and experimental studies (Ma et al., 2015; Kumar & Narayanan, 2022). Similarly, the relatively improved lift characteristics of thinner configurations can be associated with milder pressure gradients that delay boundary-layer growth and maintain favourable flow conditions over a larger portion of the chord.

The comparatively small variation in aerodynamic efficiency across the investigated thickness range suggests that thickness alone is not the dominant parameter governing lift-to-drag performance under subsonic conditions. This observation aligns with previous studies that emphasise the stronger influence of camber distribution and pressure recovery strategies in aerodynamic optimisation (Harris, 1981; Gregory & O'Reilly, 1973). From a design perspective, these findings indicate that moderate variations in airfoil thickness can be implemented to satisfy structural or manufacturing constraints without significantly compromising aerodynamic efficiency in laminar-flow-sensitive regimes. However, the sensitivity of drag behaviour to pressure-gradient development highlights the importance of accurately capturing transition effects in numerical simulations, particularly during early-stage design evaluations.

It is also important to recognise the limitations of the present study. The analysis was restricted to two-dimensional flow conditions and idealised surface characteristics, and therefore does not account for three-dimensional effects such as spanwise flow, crossflow instabilities, and surface roughness. Additionally, the transition modelling approach, although suitable for capturing relative trends, introduces uncertainties in predicting exact transition onset locations.

Despite these limitations, the controlled parametric framework adopted in this study provides valuable insights into the aerodynamic sensitivity to airfoil thickness and demonstrates the effectiveness of combined XFLR5 and CFD approaches for preliminary airfoil design and analysis. Similar thickness-sensitive aerodynamic trends have also been reported for symmetric NACA airfoils by Tunca (2025).

4.6 CFD Flow-Field Interpretation

The aerodynamic performance trends identified in the XFLR5 thickness analysis were further interpreted through the CFD flow-field visualization of the baseline NACA 0012 configuration.

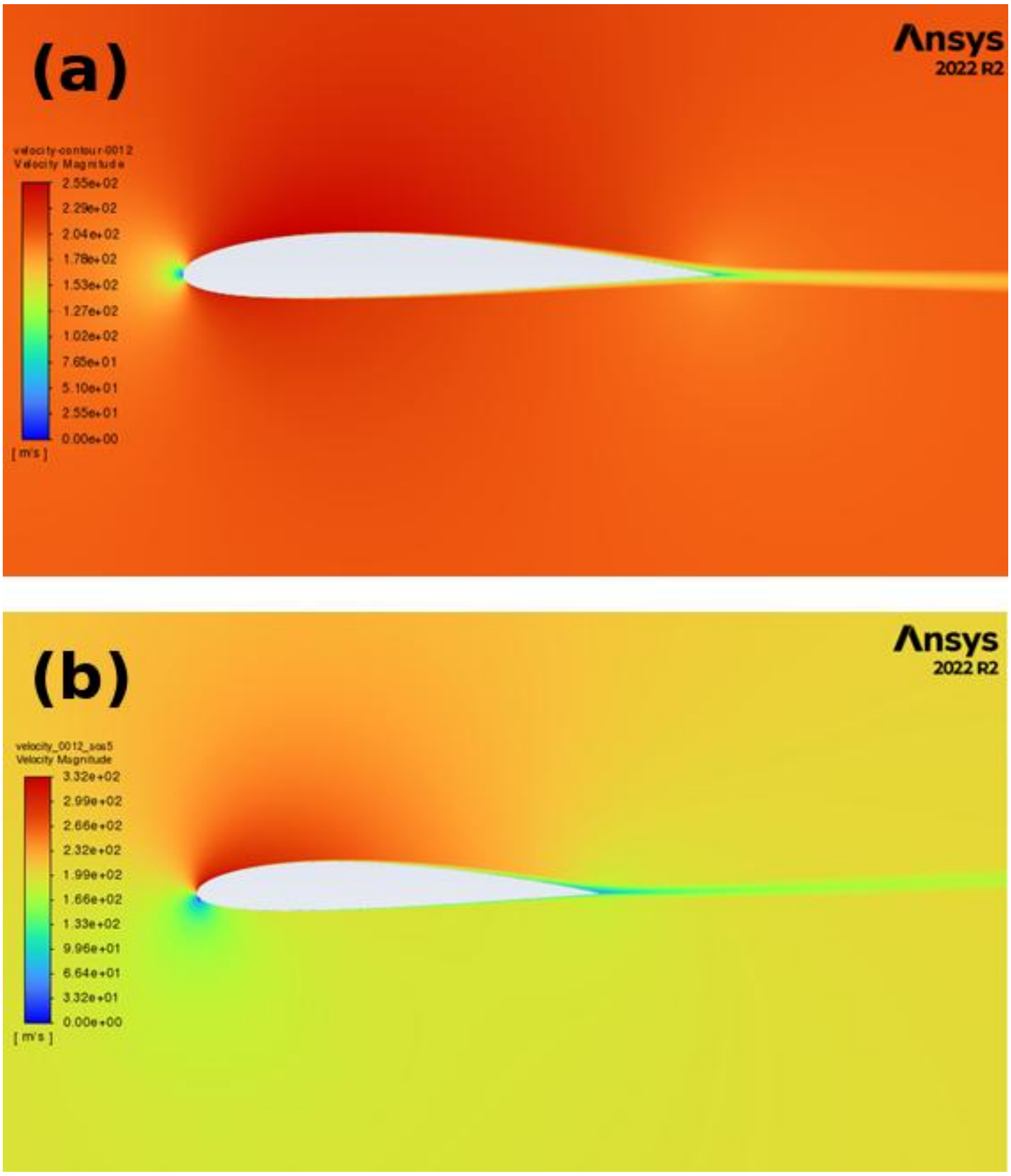

Fig. 7 Velocity magnitude contours around the NACA 0012 airfoil under subsonic conditions: (a) α = 0° and (b) α = 5°. The contours illustrate near-wall flow acceleration, wake development, and changes in velocity distribution with increasing angle of attack.

To support the interpretation of the aerodynamic performance trends, the velocity magnitude contours obtained from the CFD simulations were examined. Fig. 12 presents the velocity magnitude contours around the NACA 0012 airfoil at α = 0° and 5°.

At zero angle of attack, the flow exhibited a relatively uniform acceleration around the airfoil with a thin wake region downstream. At α = 5°, increased flow acceleration on the suction surface and a more pronounced wake structure were observed, similar wake-growth trends at low Reynolds numbers have also been reported by Chang et al. (2022). These changes indicate enhanced boundary-layer deceleration and increased wake thickness with increasing angle of attack. The observed velocity field behavior provides physical support for the drag and efficiency trends identified in Sections 4.2 and 4.3.

Fig. 13 shows the static pressure contours around the NACA 0012 airfoil at α = 0° and 5°. At zero angle of attack, the pressure distribution was relatively symmetric, with mild pressure gradients along the chord. At α = 5°, a pronounced suction region developed near the leading edge, followed by pressure recovery along the suction surface.

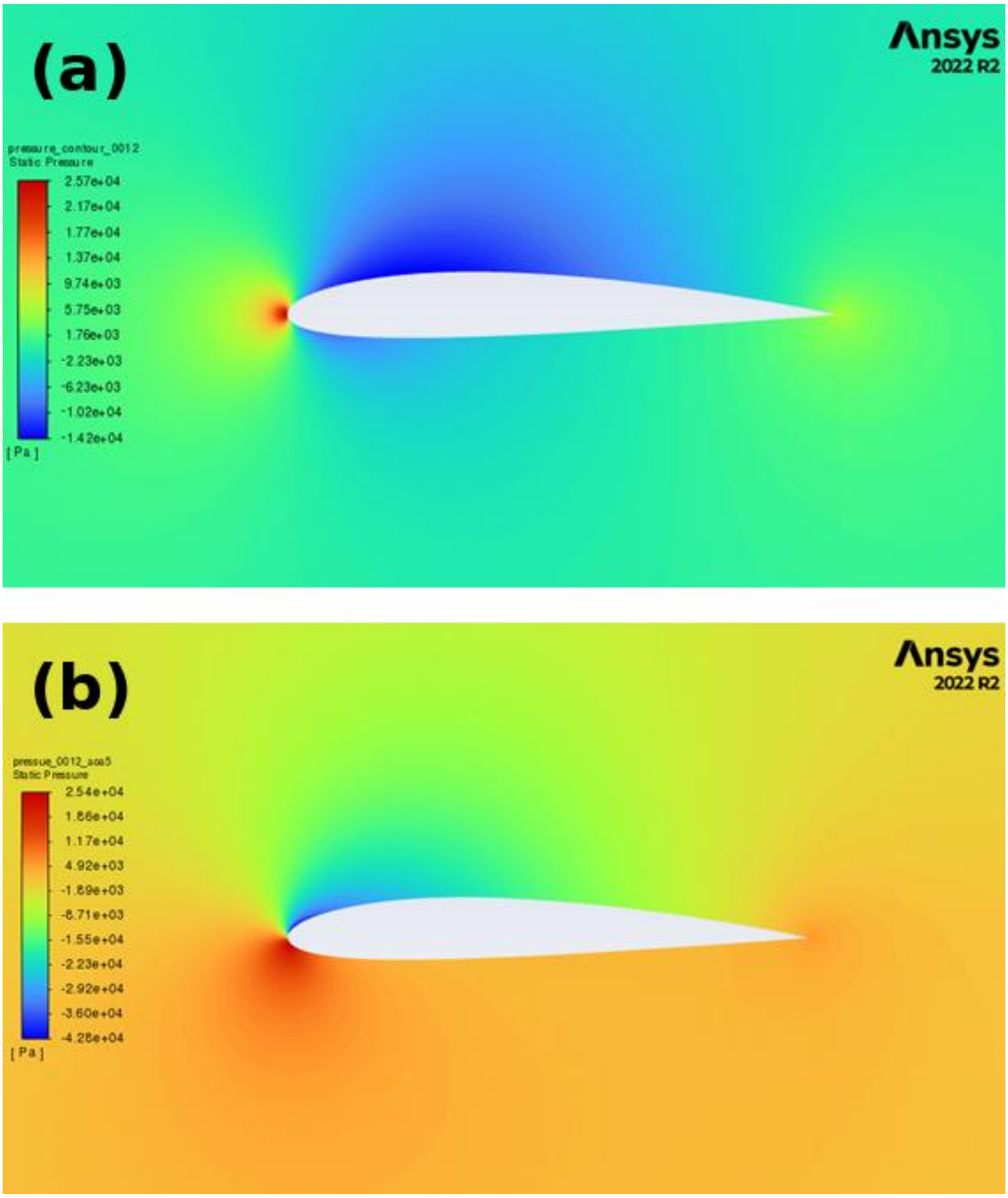

Fig. 8 Static pressure contours around the NACA 0012 airfoil under subsonic conditions: (a) α = 0° and (b) α = 5°. The contours illustrate suction-side pressure development, pressure recovery along the chord, and changes in pressure-gradient strength with increasing angle of attack.

The strengthening of adverse pressure gradients with increasing angle of attack contributes to increased boundary-layer sensitivity and drag rise. These pressure-field characteristics provide a physical explanation for the trends observed in the aerodynamic performance results and illustrate the role of pressure recovery in laminar-flow-sensitive airfoil behavior.

Fig. 14 shows the qualitative indications of the boundary layer development and turbulence-related flow features. The contours highlight regions of increased turbulence activity and boundary layer growth near the airfoil surface and in the wake.

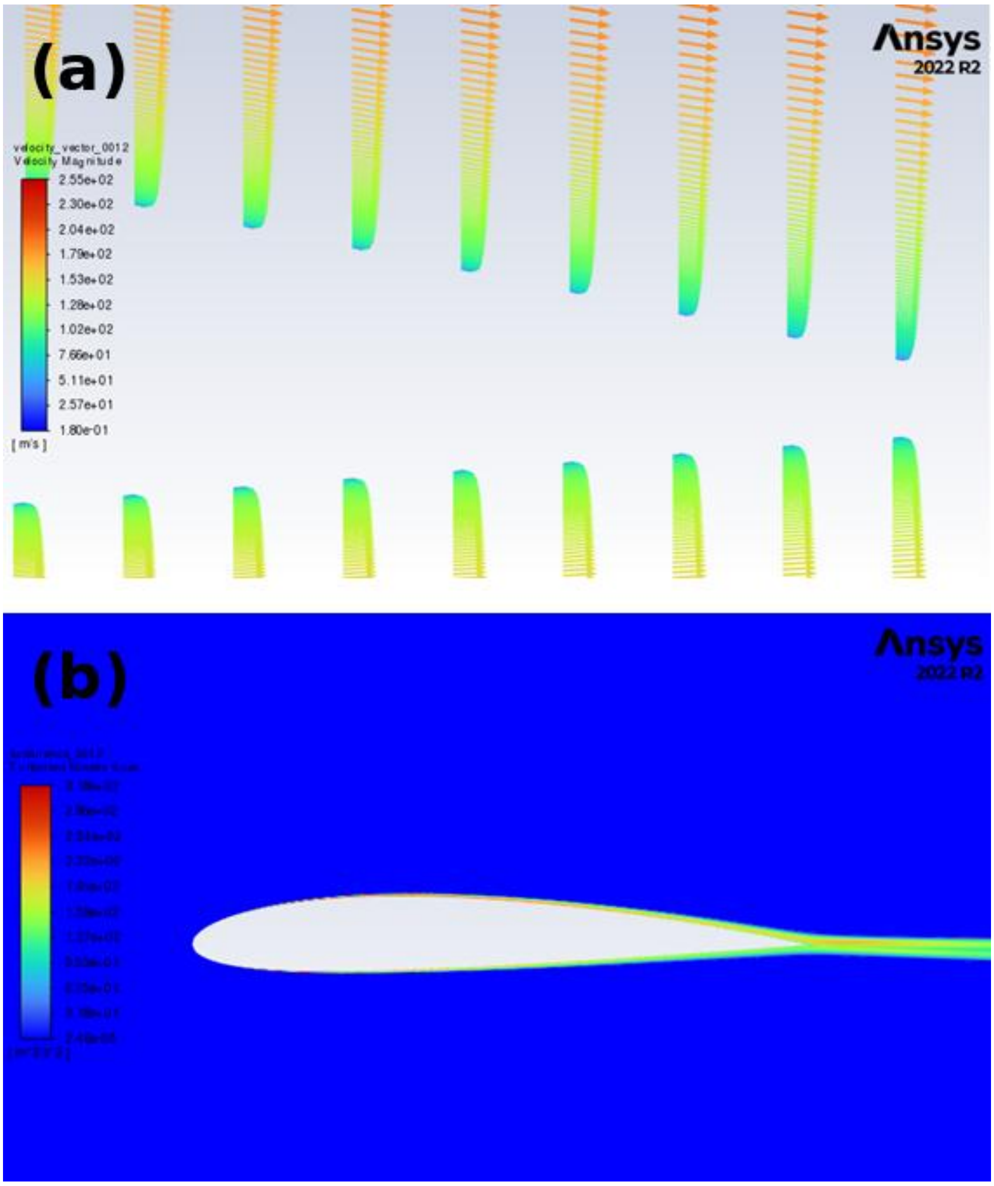

Fig. 9 Qualitative flow-field features around the NACA 0012 airfoil under subsonic conditions: (a) velocity vector field illustrating near-wall flow direction and wake development, and (b) turbulence-related contour highlighting boundary-layer growth and near-surface flow behavior.

While the precise location of laminar–turbulent transition depends on the turbulence and transition modeling approach, the relative trends indicate increasing boundary-layer thickness and turbulence levels with increasing aerodynamic loading. These features are consistent with the observed drag increase and reduction in aerodynamic efficiency at higher angles of attack.

Fig. 15 shows representative velocity vector fields obtained from the CFD simulations, providing qualitative insights into the flow direction, near-wall acceleration, and wake development behind the airfoil. The vector patterns illustrate the flow turning around the airfoil and the formation of a wake region downstream.

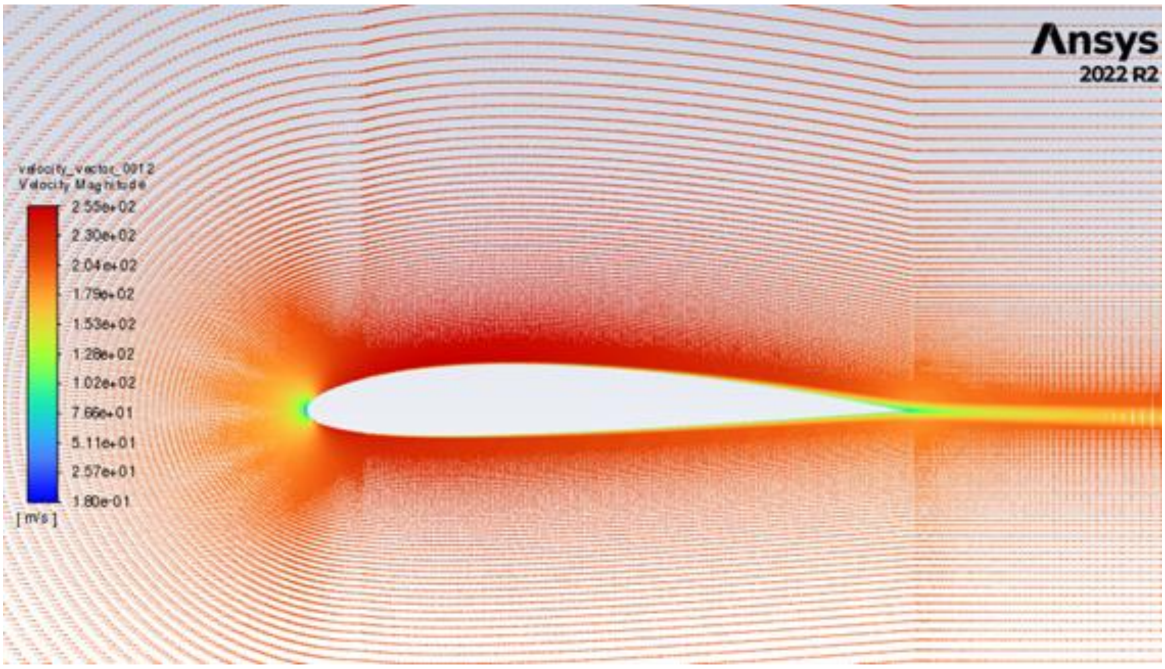

Fig. 10 Velocity vector field around the NACA 0012 airfoil illustrating flow direction, near-wall acceleration, and wake development under subsonic conditions.

The wake structure became more pronounced under higher aerodynamic loadings, indicating increased momentum deficit and energy loss. These flow-field visualizations help reinforce the interpretation that the aerodynamic performance is strongly influenced by the pressure-gradient development and boundary-layer response under subsonic conditions.

5. Conclusions

This study provided a numerical investigation into the influence of airfoil thickness on laminar-flow-sensitive aerodynamic behavior under subsonic conditions. A baseline NACA 0012 airfoil was analyzed along with the thickness-scaled variants (T090 and T110) to isolate the aerodynamic influence of thickness variation while maintaining consistent geometric characteristics. Aerodynamic performance trends were first evaluated using XFLR5 predictions and subsequently interpreted through a CFD flow-field visualization of the baseline configuration.

The results indicate that the airfoil thickness influences the aerodynamic behavior primarily through its effect on pressure gradient development and boundary-layer response. Thinner airfoils were observed to generate slightly higher lift coefficients within the investigated pre-stall regime, whereas thicker configurations exhibited marginally lower drag growth at moderate angles of attack. Despite these differences, the overall aerodynamic efficiency remained comparable across the investigated thickness range, indicating that moderate thickness variations had a relatively minor influence on the lift-to-drag performance under the analyzed operating conditions.

While the lift characteristics remained relatively robust across the investigated range, the drag behavior and aerodynamic efficiency were strongly influenced by the pressure gradient development and boundary-layer response. These results highlight the importance of accurately capturing the laminar-flow-sensitive aerodynamic behavior when analyzing the airfoil performance in preliminary design studies.

The findings highlight the sensitivity of the laminar-flow-dependent aerodynamic performance to geometric thickness variation and demonstrate the efficacy of the XFLR5 analysis and CFD approaches for early-stage airfoil analysis. The methodology adopted in this study provides a practical framework for evaluating aerodynamic design sensitivities during the preliminary aircraft design stages.

Acknowledgement

The authors would like to acknowledge Cranfield University for providing the academic environment, computational resources, and institutional support necessary for conducting this research. The guidance and facilities offered by the Faculty of Engineering and Applied Sciences are gratefully appreciated.

References

[1] Anderson, J. D. (2017). *Fundamentals of aerodynamics* (6th ed.). McGraw-Hill.
[2] ANSYS Inc. (2021). *ANSYS Fluent theory guide*. ANSYS Inc.
[3] Ruiz, M. C., & D'Ambrosio, D. (2022). Validation of the γ-Reθ transition model for airfoils operating in the very low Reynolds number regime. Flow, Turbulence and Combustion, 109, 279–308. https://doi.org/10.1007/s10494-022-00331-z
[4] Kumar, S., & Narayanan, S. (2022). Airfoil thickness effects on flow and acoustic characteristics. Alexandria Engineering Journal, 61(6), 4679–4699. https://doi.org/10.1016/j.aej.2021.10.022
[5] Ma, D., Zhao, Y., Qiao, Y., & Li, G. (2015). Effects of relative thickness on aerodynamic characteristics of airfoil at a low Reynolds number. Chinese Journal of Aeronautics, 28(4), 1003–1015. https://doi.org/10.1016/j.cja.2015.05.012
[6] Pope, S. B. (2015). *Turbulent flows*. Cambridge University Press.
[7] Matyushenko, A. A., Stabnikov, A. S., & Garbaruk, A. V. (2018). Comparative analysis of transition models in prediction of flow over NACA-0012 airfoils in tandem. Journal of Physics: Conference Series, 1038, 012130. https://doi.org/10.1088/1742-6596/1038/1/012130
[8] Shah, H., Mathew, S., & Lim, C. M. (2015). Numerical simulation of flow over an airfoil for small wind turbines using the γ-Reθ model. International Journal of Energy and Environmental Engineering, 6, 419–429. https://doi.org/10.1007/s40095-015-0188-7
[9] Khan, S. A., Bashir, M., Baig, M. A. A., & Ali, F. A. G. M. (2020). Comparing the effect of different turbulence models on the CFD predictions of NACA0018 airfoil aerodynamics. CFD Letters, 12(3), 1–10. https://doi.org/10.37934/cfdl.12.3.110
[10] Tunca, S. G. (2025). Analysis of flow separation and aerodynamic behavior on NACA0012 and NACA0015 airfoils. Karamanoğlu Mehmetbey University Journal of Engineering and Natural Sciences, 7(2), 88–98. https://doi.org/10.55213/kmujens.1824626
[11] Bangga, G., Hutami, S., & Hernawan, H. (2021). The effects of airfoil thickness on dynamic stall characteristics of high-solidity vertical axis wind turbines. Advanced Theory and Simulations, 4(6), 2000204. https://doi.org/10.1002/adts.202000204
[12] Nandi, T. N., Brasseur, J. G., & Vijayakumar, G. (2016). Prediction and analysis of the nonsteady transition and separation processes on an oscillating wind turbine airfoil using the γ-Reθ transition model. AIAA SciTech 2016.
[13] Critzos, C. C., Heyson, H. H., & Boswinkle Jr., R. W. (1955). Aerodynamic Characteristics of NACA 0012 Airfoil Section at Angles of Attack from 0° to 180°. NACA Technical Note 3361.
[14] Gregory, N., & O'Reilly, C. L. (1973). Low-Speed Aerodynamic Characteristics of NACA 0012 Aerofoil Section, including the Effects of Upper-Surface Roughness Simulating Hoar Frost. Aeronautical Research Council Reports and Memoranda No. 3726.
[15] Chang, J., Zhang, Q., He, L., & Zhou, Y. (2022). Shedding vortex characteristics analysis of NACA 0012 airfoil at low Reynolds numbers. Energy Reports, 8, 156–174. https://doi.org/10.1016/j.egyr.2022.01.149

[16] Güzelbey, İ. H., Eraslan, Y., & Doğru, M. H. (2018). Numerical Investigation of Different Airfoils at Low Reynolds Number in terms of Aerodynamic Performance of Sailplanes by using XFLR5. Karadeniz Fen Bilimleri Dergisi, 8(1), 47–65.
[17] Harris, C. D. (1981). Two-Dimensional Aerodynamic Characteristics of the NACA 0012 Airfoil in the Langley 8-Foot Transonic Pressure Tunnel. NASA Technical Memorandum 81927.
[18] Douvi, E. C., Tsavalos, A. I., & Margaris, D. P. (2010). CFD Calculations of the Flow Over a NACA0012 Airfoil. Proceedings of the 4th IC-SCCE.
[19] Jha, S., Gautam, U., Narayanan, S., & Dhas, L. A. K. (2018). Effect of Reynolds Number on the Aerodynamic Performance of NACA0012 Aerofoil. IOP Conference Series: Materials Science and Engineering, 377, 012129.
[20] Kim, D.-H., Chang, J.-W., & Sohn, M. H. (2017). Unsteady Aerodynamic Characteristics depending on Reduced Frequency for a Pitching NACA0012 Airfoil at Rec = 2.3×10^4. International Journal of Aeronautical and Space Sciences, 18(1), 8–16.
[21] Zidane, I. F., Swadener, G., Saqr, K. M., Ma, X., & Shehadeh, M. F. (2017). CFD Investigation of Transitional Separation Bubble Characteristics on NACA 63415 Airfoil at Low Reynolds Numbers. Proceedings of the 25th UKACM Conference on Computational Mechanics, University of Birmingham, UK.